WORLD CONFERENCE ON TIMBER ENGINEERING 2025
BRISBANE, AUSTRALIA
Advancing Timber for the Future Built Environment

INVESTIGATIONS ON STEEL-TIMBER-CONCRETE COMPOSITE SHALLOW FLOOR BEAMS: COMPARISON BETWEEN STRAIN-BASED DERIVED BENDING RESISTANCES AND RESULTS OF NUMERICAL MODELS

Adil Ahmad[1], Christoph Odenbreit[2], Jean-François Demonceau[3], Jie Yang[4]

ABSTRACT: To limit the emission of greenhouse gases, the 'Green Deal' and the Taxonomy Regulation were introduced in the European Union. This inevitably leads to a change in the construction industry, with the aim of reducing carbon dioxide emissions to (net) zero by 2050. The development and use of constructional timber can also be purposeful. For steel construction, this means expanding the composite construction method from steel-concrete to steel-timber and possibly also steel-timber-concrete composites. In this contribution the steel-timber-concrete composite shallow floor beams are investigated, which reduce the floor height and enable either a reduction of the height of the building or in the construction of more floors. Here the steel sheet and most of the concrete of traditional steel-concrete beams are replaced by timber. This change in material results in a different load bearing behaviour and different characteristics which need to be reflected in the overall bending capacity. The paper shows the results on the investigation about steel-timber-concrete composite shallow floor beams using a strain limited approach and compares these to the results of numerical models using the finite element software ABAQUS©. It suggests that the strain-based method can be a viable approach to assess the bending capacity of steel-timber-concrete shallow floor beams.

KEYWORDS: timber, composite, steel, shallow floor beam, strain-controlled

1 – INTRODUCTION

The practice of replacing traditional construction materials with alternatives that have a lower impact on global warming is becoming increasingly common, especially in current research. Romero [1;2] analysed the replacement of concrete in classic steel-concrete composite beams with a timber slab. To analyse the bending moment capacity of steel-timber composite (STC) beams, a strain-based approach is used. It is important to note that Romero's beam, as well as most other analysed timber-composite beams, had vertically stacked materials.

Vertically and horizontally layered composite beams

The strain-based analysis of the steel-timber-concrete composite (STCC) shallow floor beam investigated in this paper (Fig.3) is more sophisticated since three materials are used, which are not only stacked vertically but also horizontally resulting in the neutral fibres of the timber and steel being approximately on the same level. The concrete, which is laying on top of both components (timber and steel) acts with both materials through a composite action. So, shear is activated between steel-timber, steel-concrete and concrete-timber. Therefore, the present study investigates if the strain-based analysis can be adapted to assess the bending moment capacity of such STCC shallow floor beams or multilayered, multi-material composites and compares the results to those of numerical models.

2 – STRAIN-BASED DETERMINATION OF BENDING RESISTANCE

For timber beams Eurocode EN1995-1-1 is applied. But since EN1995-1-1 requires an elastic analysis approach it is not suitable for composite beams, where other components or materials can develop plasticity. As there is no design guide for steel-timber composites, a strain-based method was used to analyse the bending moment capacity of the section and, consequently, of the beam.

2.1 GENERAL

The method uses the strain limits of the components, i.e. steel and timber and analyses the strain distribution over

[1] Adil Ahmad, University of Luxembourg, Esch-sur-Alzette, Luxembourg, adil.ahmad@uni.lu

[2] Christoph Odenbreit, University of Luxembourg, Esch-sur-Alzette, Luxembourg, christoph.odenbreit@uni.lu

[3] Jean-François Demonceau, University of Liège, Liège, Belgium, jfdemonceau@uliege.be

[4] Jie Yang, R&D ArcelorMittal, Esch-sur-Alzette, Luxembourg, jie.yang@arcelormittal.com

https://doi.org/10.52202/080513-0548

the cross-section (where the slab is of timber and the beam is out of steel). Following EN1994-1-1, 6.2.1.3 [11], first the bending moment capacity of the composite beam must be analysed with no degree of shear connection (η=0). EN1994-1-1 simplifies the first step through using the plastic bending moment capacity of just the steel beam alone (Mpl,a,R), though this will not be used here, as the top slab also contributes to the capacity. In this state (η=0) the materials act by themselves and follow the same strain gradient around their neutral axis (Fig. 1).

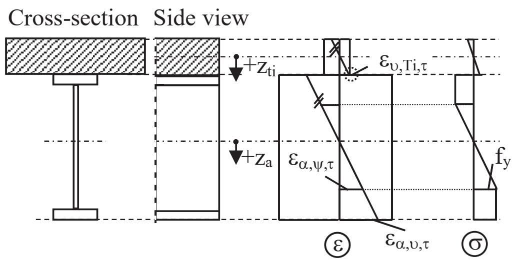

Figure 1: Example of the strain and stress distribution for a composite beam with no shear connection (η=0)

The bending capacity is calculated as (1):

$$M_{\eta 0}= \int_{A_{ti}} \sigma(z)\cdot z_{ti}\, dA_{ti} + \int_{A_a} \sigma(z)\cdot z_a\, dA_a \tag{1}$$

where:

A_{ti}, z_{ti} Area and lever arm of the timber slab

A_a, z_a Area and lever arm values of the steel beam

To assess the upper limit of the composite beam (full shear connection, η=1), the strain distribution is assumed to be linear over the whole section. Taking the boundary limit of the timber slab in compression as a hinge point, the strain distribution line is then tilted along the strain limit of the steel in tension. The strain limit of the timber in tension ($\varepsilon_{ti,u,t}$) is not to be exceeded. In the rare case of the steel strain limit in tension being reached, the hinge switches from the timber to the steel strain limit. When the forces over the section are in equilibrium through adjusting the strain distribution line, they are integrated to derive the bending moment capacity (Figure 2 and (2)).

$$M_{\eta 1}= \int_A \sigma(z)\cdot z\, dA \tag{2}$$

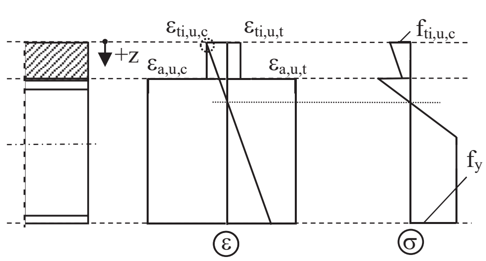

Figure 2: Example of the strain and stress distribution for composite beam with full shear connection (η=1)

As a last point, the composite beams bending moment capacity is assessed in partial shear connection (0<η<1). The shear connector capacity (P_R) enables the calculation of the transferable compressive force from the slab to the beam ($N_{c,\eta}$). It is calculated as (3) and limited by $N_{c,\eta 1}$:

$$P_R n = N_{c,\eta} < N_{c,\eta 1} = \int_{A_{ti}} \sigma(z)\, dA_{ti} \tag{3}$$

Adjusting the strain in the timber slab and then correcting the strain position in the beam allows us to derive the bending moment capacity under partial shear connection.

2.2 STCC SHALLOW FLOOR BEAM

Since in most shallow floor beams the sections are not stacked purely vertically, but also horizontally, the strain-based method needs to be adjusted. This paper, as a first step, analyses the horizontal shear planes of the section as in full shear (η=1). The approach is the same as in Figure 2. The layout of the analysed STCC shallow floor beam is as follows: In the middle is a concrete filled steel beam, while on the sides Cross-laminated timber (CLT) panels acts as the floor slabs. The CLT and the steel profile are connected via a concrete slab laying on top of them, enabling a composite action through an unspecified full shear connection (Fig. 3).

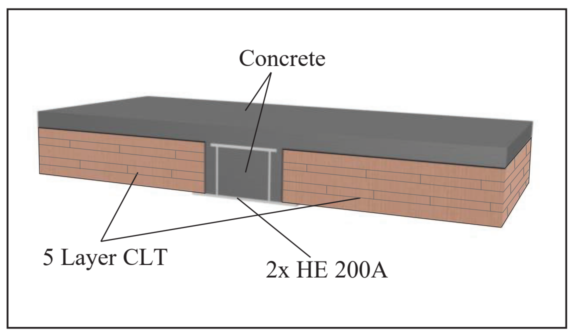

Figure 3: Steel-timber-concrete composite shallow floor beam layout

The boundary limit of the cross-section in the top is limited by the concrete ($\varepsilon_{c,u,c}$; $\varepsilon_{c,u,t}$). Since the timber and steel must deform at the same rate, the material with the smaller strain sets the boundaries of the lower cross-section. As such the strain boundaries will look according to Fig. 4.

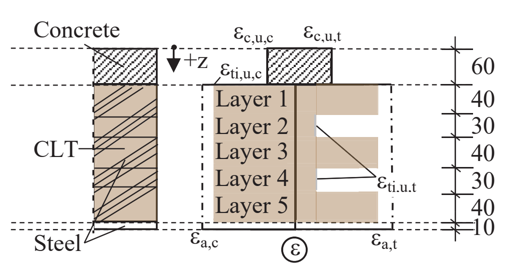

Figure 4: Strain boundaries of the analysed STCC shallow floor beam

https://doi.org/10.52202/080513-0548

3 – PARAMETRIC STUDY

3.1 OVERVIEW ON INVESTIGATED BEAMS

The geometry of the beams is shown in Fig. 3 while the material and their strength were varied. A designation was given to each investigated beam, where the first number of the designation indicates the steel grade (e.g. 2 = S235), the following letter indicates the timber used (e.g. C = CLT - C24, B = CLT - Beech) and the last two numbers indicate the concrete class (e.g. 20 = C20/25). An overview is provided in Table 1.

TABLE 1: OVERVIEW ON INVESTIGATED BEAMS

Designation	Characteristics		
	Steel	***Timber***	***Concrete***
2C20	S235	CLT – C24	C 20/25
3C20	S355	CLT – C24	C 20/25
4C20	S460	CLT – C24	C 20/25
2C30	S235	CLT – C24	C 30/37
3C30	S355	CLT – C24	C 30/37
4C30	S460	CLT – C24	C 30/37
2C45	S235	CLT – C24	C 45/55
3C45	S355	CLT – C24	C 45/55
4C45	S460	CLT – C24	C 45/55
2B20	S235	CLT – Beech	C 20/25
3B20	S355	CLT – Beech	C 20/25
4B20	S460	CLT – Beech	C 20/25
2B30	S235	CLT – Beech	C 30/37
3B30	S355	CLT – Beech	C 30/37
4B30	S460	CLT – Beech	C 30/37
2B45	S235	CLT – Beech	C 45/55
3B45	S355	CLT – Beech	C 45/55
4B45	S460	CLT – Beech	C 45/55

The values for the CLT – C24 were taken from the technical specification of KLH® [3]. Spruce is being used as the timber source material. Additionally, the beams were investigated with CLT consisting of beech wood instead of spruce [4]. Since timber in compression exhibits non-linear ductile behaviour, this plastic potential was considered using the Hill yield criterion [5]. Since the timber is mostly under tension in this configuration and the strain-controlled analysis sets the boundaries through the strain limits, it would be acceptable to leave out the modelling of plasticisation of the timber. Fig. 5 shows the dimensions of the cross-section.

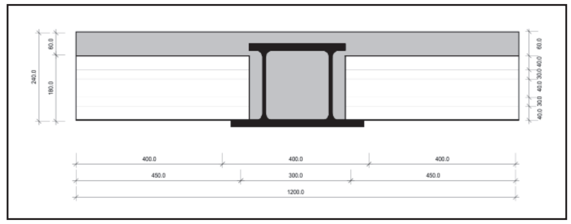

Figure 5: Dimensions of the cross-section of the shallow floor beam

3.2 THE STRAIN-CONTROLLED ANALYSIS

Using the method described in Section 2, the cross-section was divided into the different materials. Per material the geometry was partitioned into separate rectangles and then divided into small layers (in this case into 1/100 of the height of the partition) Fig. 6 shows the example of the partitioning for concrete and steel.

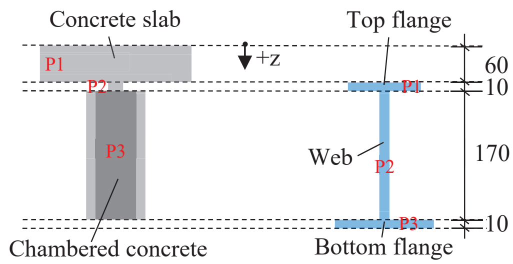

Figure 6: Partitioning of the concrete (left) and steel (right)

Since mainly the second and fourth layer of the CLT contribute to the bending moment capacity, the other layers will be ignored during the analytical assessment. Once the strain boundaries are set, a linear strain distribution will be set. Integrating the stresses of each layer over the height and adjusting the inclination and position of the strain distribution to achieve equilibrium of the forces, the bending moment can then be assessed.

Fig. 7 shows the strain boundaries for the exemplary beam 4C20.

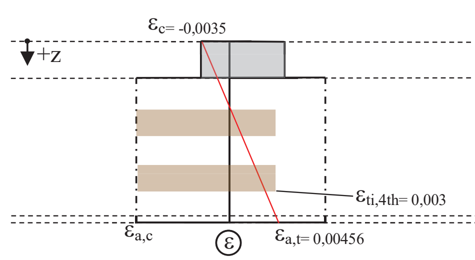

Figure 7: Strain distribution of the 4C20 STCC shallow floor beam

https://doi.org/10.52202/080513-0548

Table 2 presents the analytically obtained results of the beams including the strain in the uppermost layer of the concrete, the strain in the bottom flange of the steel beam, and the resulting bending moment capacity at the maximal deflection. The deflection was calculated by the second integral of the curvature (obtained by the inclination of the strain distribution), assuming a sine deflection.

TABLE 2: OVERVIEW - STRAIN BASED METHOD

Beam	*Strains*		*Bending Moment Capacity [kNm]*	*Deflection [mm]*
	Top strain (z=0mm)	*Bottom strain (z=250mm)*		
2C20	-2,76 ‰	5,82 ‰	359,61	97,85
3C20	-3,50 ‰	5,60 ‰	448,27	103,65
4C20	-3,50 ‰	4,56 ‰	509,93	91,88
2C30	-2,29 ‰	5,71 ‰	378,44	91,14
3C30	-2,88 ‰	5,85 ‰	490,77	99,54
4C30	-3,50 ‰	5,96 ‰	572,09	107,82
2C45	-1,99 ‰	5,63 ‰	394,97	86,87
3C45	-2,37 ‰	5,73 ‰	516,21	92,28
4C45	-2,73 ‰	5,82 ‰	616,31	97,41
2B20	-3,50 ‰	7,62 ‰	402,79	126,73
3B20	-3,50 ‰	6,13 ‰	496,86	109,7
4B20	-3,50 ‰	5,15 ‰	572,13	92,28
2B30	-3,50 ‰	9,12 ‰	434,74	143,75
3B30	-3,50 ‰	7,47 ‰	535,80	125,02
4B30	-3,50 ‰	6,35 ‰	617,83	98,52
2B45	-3,11 ‰	9,56 ‰	464,73	144,40
3B45	-3,50 ‰	4,60 ‰	604,62	92,28
4B45	-3,50 ‰	7,04 ‰	552,07	120,10

3.3 NUMERICAL SIMULATIONS

To assess the strain-method derived bending moment capacities from section 3.2, a numerical non-linear 3D model was created using the finite element (FE) software ABAQUS©.

Since an experimental test with a configuration as described in section 2 and 3 is planned, the validation of the numerical model was estimated through comparison of steel concrete composite beams [6] and steel timber composite beams [1]. Consequently, the complete validation (with specification to partial shear connection) and the comparison of an experimental vs. numerical model will be presented in a future article, following the experimental test campaign.

The objective of the numerical models is to verify that the maximum bending capacity of the strain-controlled analysis is in good compliance with the results obtained through FE-Analysis.

Modelling description

A dynamic-explicit solver was used to avoid convergence issues that may occur during separation and plasticisation of components. Mass-scaling was applied as well. All parts were modelled as beam elements, where the front faces of the components were sketched and then extended.

The CLT was modelled as a five-layer stacked block of two single timber pieces, where the piece running parallel to the beam was modelled as a 2x 2,625m long and 0,15m wide piece. The piece perpendicular to the steel beam had a length of 0,45m and a width of 0,2625m. As such, the CLT block had the dimensions (L/W/H) of 5,25/0,45/0,18m^3.

According to the L, T, R dimension scheme from section 3.1 table 2 for timber, the orientation of the two timber pieces was also changed to comply with the material characteristics used.

Figure 9 shows the numerical model in the graphical user interface (GUI) of the FE-Software ABAQUS©.

Material characteristics

The following figures show the strain-stress curves of the used material:

Timber (Fig. 8):

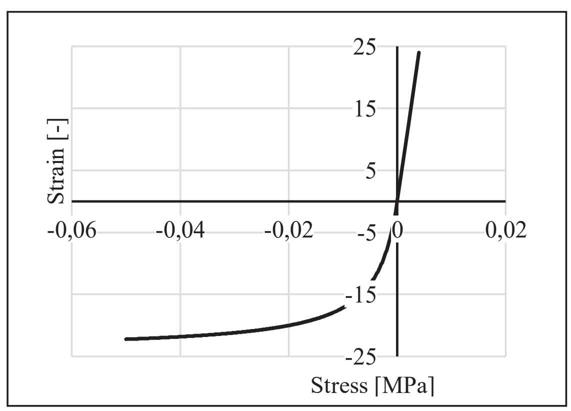

Figure 8: Timber material law for the beam 4C20

The plasticisation of the wood was modelled using the potential function in ABAQUS© and applying the Hill yield criterion according to the formulation (4):

https://doi.org/10.52202/080513-0548

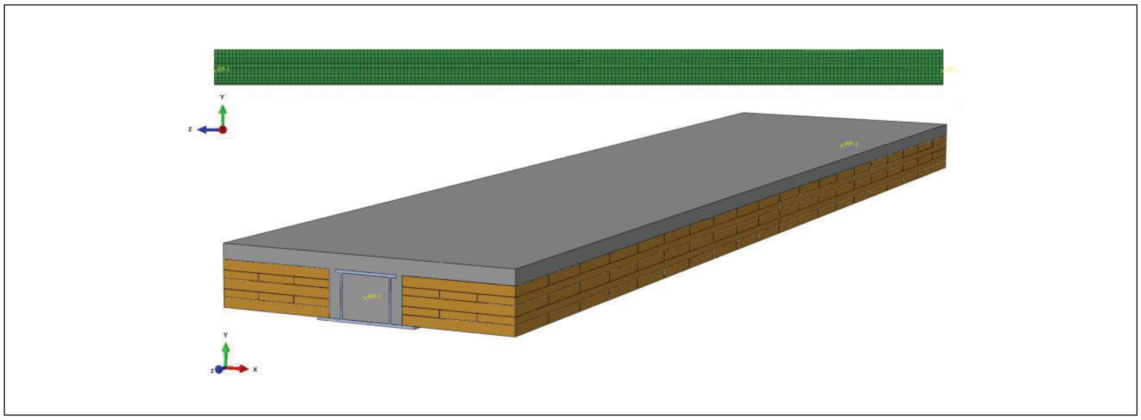

Figure 9. Numerical model of the composite beam in the FE-software Abaqus©, mesh (top), Material visual representation (bottom)

$$F(\sigma_{22}\text{-}\sigma_{33})^2 + G(\sigma_{33}\text{-}\sigma_{11})^2 + H(\sigma_{11}\text{-}\sigma_{22})^2$$

$$+ 2L\sigma^2{}_{23} + 2M\sigma^2{}_{31} + 2N\sigma^2{}_{12} = 1 \quad (4)$$

where:

$$F = \frac{1}{2}\left(\frac{1}{R_{22}^2} + \frac{1}{R_{33}^2} + \frac{1}{R_{11}^2}\right) \quad (5)$$

$$G = \frac{1}{2}\left(\frac{1}{R_{33}^2} + \frac{1}{R_{11}^2} + \frac{1}{R_{22}^2}\right) \quad (6)$$

$$H = \frac{1}{2}\left(\frac{1}{R_{11}^2} + \frac{1}{R_{22}^2} + \frac{1}{R_{33}^2}\right) \quad (7)$$

$$L = \frac{3}{2R_{23}^2} \quad (8)$$

$$M = \frac{3}{2R_{13}^2} \quad (9)$$

$$N = \frac{3}{2R_{12}^2} \quad (10)$$

The values for $R_{11}, R_{22}, R_{33}, R_{12}, R_{13}, R_{23}$ are listed in table 3.

TABLE 3: TIMBER CHARACTERISTICS

Characteristic	Specification	CLT - C24	CLT - Beech
E-modulus	L(ongitudinal)	6000	14788
	R(adial)	810	1848
	T(angetial)	363	1087
G-modulus	LR	811	1260
	LT	788	971
	RT	67	366
Poisson's Ratio	LR	0,56	0,39
	LT	0,68	0,46
	RT	0,54	0,67
Yield stress ratio	R11	1	1
	R22	0,1125	0,212
	R33	0,1125	0,212
	R12	0,1949	0,233
	R13	0,0866	0,15
	R23	0,0866	0,15

No subroutine was used, which enables the configuration of elastic-plastic (ductile) compression and an elastic-elastic (tension) material law within the finite element software ABAQUS© [7,8]. This is because the strain in tension was limited by the preliminary estimation using the strain-controlled method and basing it on the condition, that timber shall not crack according to EN1995 [12].

For steel the material law described in the Eurocode EN1993-1-1 [10] was used. A bilinear curve was applied, incorporating strain hardening in the plasticisation zone (fig. 10).

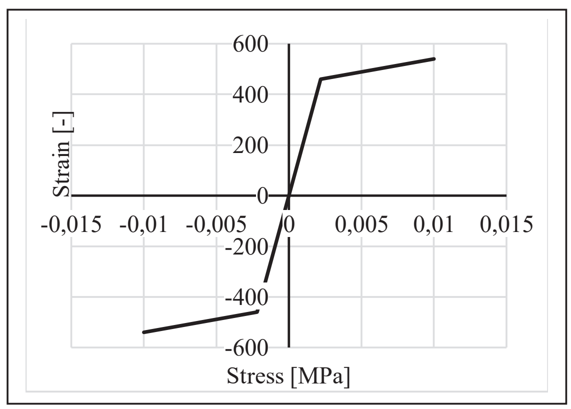

Figure 10: Steel material law for the beam 4C20

For the concrete law a parabola was used for the stress-strain relationship in compression in connection to prEN 1992-1-1, 5.1 [9] while in tension a linear relationship was defined with the maximum tensile stress estimated as 10% of the maximum compression stress. The concrete plastic damage model was applied as well (fig. 11).

https://doi.org/10.52202/080513-0548

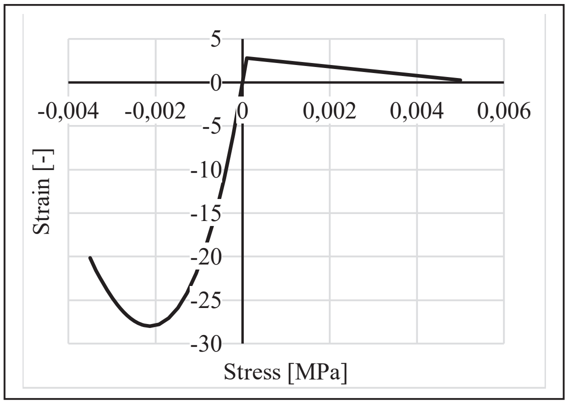

Figure 11: Concrete material law for the beam 4C20

Boundary conditions

To enable a full connection of the top concrete slab to the steel and CLT, the bottom surface of the concrete was tied to the top surfaces of the CLT and steel beam, respectively. The CLT planks were tied to each other layer by layer, as according to EN1995-1-1, 3.6, the adhesion of the layers must be characterised sufficiently to prevent failure due to the adhesive, as it must maintain the bon integrity throughout the expected lifetime of the structure.

All other connections were characterized by a global "hard" surface-to-surface contact with a friction coefficient of 0.6 to prevent surfaces from traveling through each other. The tied surfaces were specifically excluded from this global connetion.

The steel beam was pinned on one end, by holding the U1, U2 directions as well as rotations about U1 and U2 axis. On the other side the beam was supported as with a roller support, only holding the U2 direction and hindering rotation around the U1 and U2 axis, simulating a simply supported beam (fig. 12).

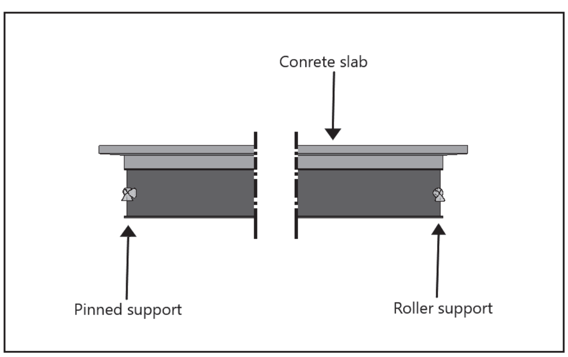

Figure 12: Scheme of the support conditions of a simple composite beam

A uniformely distributed load (UDL) was placed on top of the concrete slab, whereby the load introduction was applied using the smooth step.

Failure or model limitation

The numerical model was stopped when the beam reached a midspan deflection of 150mm. This deflection translates into L/35. It sufficiently covers the deflection limit of L/300 for normal beams, L/250 for composite beams as well as L/50 and L/40 for extreme ULS cases.

4 – COMPARISON

Below, the results of the analytically and numerically obtained valued are listed. Here, the analytically derived, strain-controlled maximal bending moment capacities and their respective deflections, obtained by estimating a sinusoidal beam deflection and using the second integral of the beam curvature (κ), are compared to the numerically derived bending moments achieved at the same deflection given by the strain-controlled method (see Table 4).

TABLE 4: OVERVIEW – COMPARISON

Beam	Bending moment capacities		
	M_{abaqus} [kNm]	*$M_{strain\text{-}controlled}$ [kNm]*	*Difference [%]*
2C20	362,82	359,61	0,89
3C20	452,36	448,27	0,91
4C20	524,20	509,93	2,80
2C30	373,12	378,44	0,52
3C30	479,39	490,77	2,32
4C30	554,11	572,09	3,14
2C45	391,62	394,97	0,85
3C45	493,48	516,21	4,40
4C45	589,11	616,31	4,41
2B20	410,14	402,79	1,83
3B20	500,29	496,86	0,69
4B20	571,93	572,13	0,04
2B30	461,74	434,74	6,21
3B30	549,78	535,80	2,61
4B30	630,61	617,83	2,07
2B45	515,21	464,73	10,86
3B45	584,23	604,62	3,37
4B45	636,04	632,47	0,56

Figure 13 show the results of the analysed beams. The moment-deflection curves are separated by their steel grade.

https://doi.org/10.52202/080513-0548

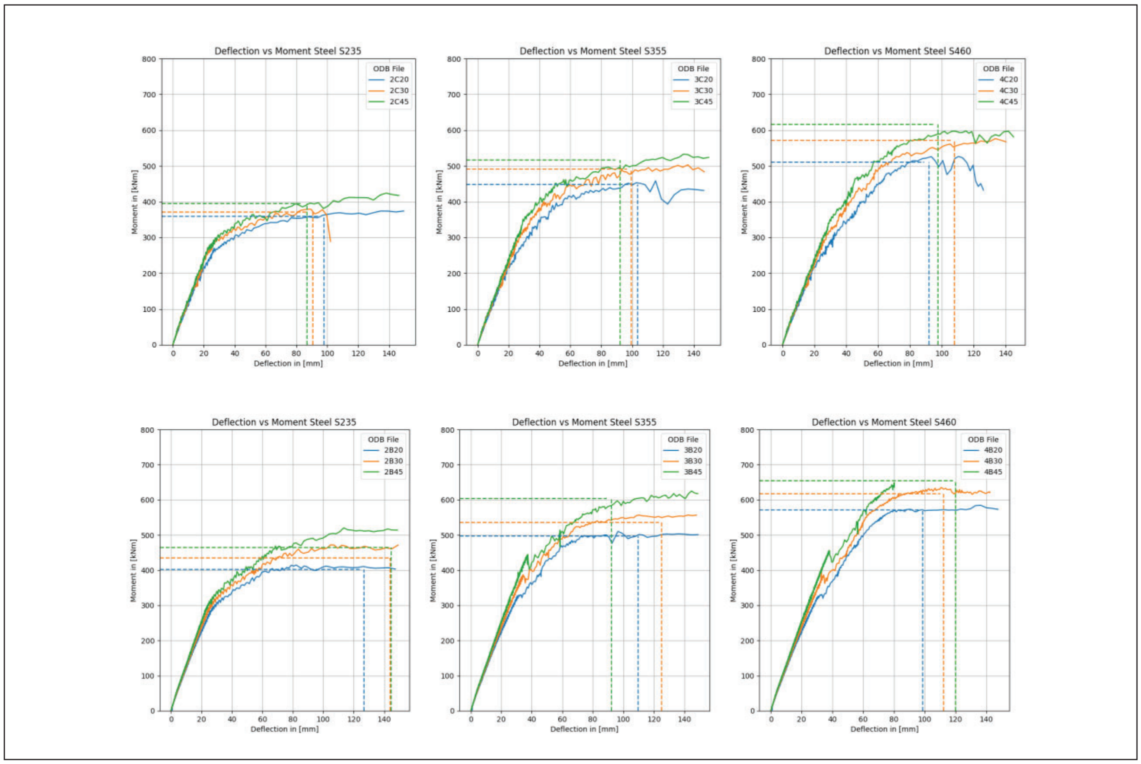

Figure 13. Moment deflection curves of the beams in comparison with the analytical estimation (dashed lines). Spruce top, beech bottom.

5 – CONCLUSION AND OUTLOOK

The comparison shows a maximal difference of 10,86% while the minimum deviation was 0,04%. The difference seems to stem from the fact, that the case just connecting the concrete slab with the steel and timber is not sufficient. Rather all shear planes shall act in a similar manner, since the strain-controlled method indicate a uniform behaviour of the cross-section. Due to the concrete compressing further in the numerical simulation, stronger forces are being generated in the slab, which in turn can increase the bending moment capacity during the simulation. Additionally, the CLT blocks rotate away from the beam. Therefore, it is recommended to also fasten the other shear planes.

Looking at the overall results it can be assumed, that the strain-controlled method to estimate the bending moment capacity works well in full shear connection. It also shows that the use of timber with higher strength positively affects the bending moment capacity since here the strain limit of the concrete did not allow the timber to develop its whole strain in tension. Also, a steel with a higher strength grade improves the bending moment capacity. It can also be said that the limiting factor of such a mutli material composite beam in this configuration is mainly the strain limitation of the timber used, which allows for further reduction of the concrete amount in the slab.

As the next step the strain-controlled method analyses the beam without any shear connection (eta=0) (following EN1994).

Using a method to estimate the shear connector capacity, the calculation of the bending moment capacity of the beam in partial shear connection becomes possible [1]. As such a moment to degree of shear connection curve can be created, at least in case of simple composite beams.

In case of a multi material composite, the differences in slip-distribution of different shear connectors and shear planes make it harder to access the bending capacity of the beam in partial shear connection.

To analyse the viablitiy and efficiency of the strain-controlled method in multi material composite beams also in partial shear connection, an experimental test will be undertaken. The challange in the estimation of the bending moment capacity for multi material composite in partial shear connection lies in the additional degrees of freedom and variables added into the analysis. As such certain conditions must be stated to simply the estimation.

https://doi.org/10.52202/080513-0548

6 – REFERENCES

[1] A. Romero "Demountable and Reusable Steel-Timber Composite beams." Doctoral Thesis, University of Luxembourg, Luxembourg, 2024.

[2] A. Romero, C. Odenbreit "Experimental Investigation on Strength and Stiffness Properties of Laminated Veneer Lumber (LVL)." Materials, 2023.

[3] KLH Massivholz GmbH. "Declaration of Performance No.: DOP_KLH_K_2021_v01_de." KLH Massivholz GmbH. Accessed March 30, 2025. https://www.klh.at/wp-content/uploads/2021/01/dop-klh-2021-v01-de.pdf.

[4] V. D. Tran, M. Oudjene, P. Méausoone "FE analysis and geometrical optimization of timber beech finger-joint under bending test" International Journal of Adhesion and Adhesives, 2014.

[5] R. Hill "A Theory of the Yielding and Plastic Flow of Anisotropic Metals." Proceedings of the Royal Society of London. Series A, Mathematical and Physical Sciences, vol. 193, no. 1033, 1948.

[6] A. Kozma "Demountable composite beams: Analytical calculation approaches for shear connections with multilinear load-slip behaviour." Doctoral Thesis, University of Luxembourg, Luxembourg, 2020.

[7] Dassault Systèmes. Abaqus, Version 2024. 2024.

[8] F. Mirianon, S. Fortino, T. Toratti "A method to model wood by using ABAQUS finite element software Part 1. Constitutive model and computational details." VTT Publications, no. 687, 2008, 51 p.

[9] European Committee for Standardization. "Eurocode 2: Design of Concrete Structures - Part 1-1: General Rules and Rules for Buildings". prEN 1992-1-1, 2024.

[10] European Committee for Standardization. "Eurocode 3: Design of Steel Structures - Part 1-1: General Rules and Rules for Buildings". EN 1993-1-1, 2005.

[11] European Committee for Standardization. "Eurocode 4: Design of Composite Steel and Concrete Structures - Part 1-1: General Rules and Rules for Buildings". EN 1994-1-1, 2004.

[12] European Committee for Standardization. "Eurocode 5: Design of Timber Structures - Part 1-1: General Rules and Rules for Buildings". EN 1995-1-1, 2004.

7 – ACKNOWLEDGEMENT

The authors extend their sincere gratitude to ArcelorMittal Luxembourg for their invaluable support in the AM-SeTi research project.

https://doi.org/10.52202/080513-0548